Journal Pre-proofs

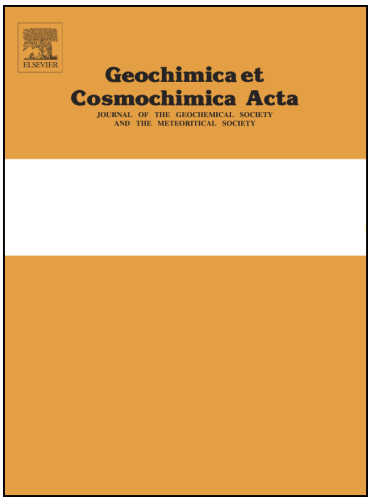

Effects of organic matter complexation on partitioning of transition metals into calcite: Cave-analogue crystal growth experiments

I. Lindeman, M. Hansen, D. Scholz, S.F.M. Breitenbach, A. Hartland

PII: S0016-7037(21)00645-1
DOI: https://doi.org/10.1016/j.gca.2021.10.032
Reference: GCA 12434

To appear in: *Geochimica et Cosmochimica Acta*

Received Date: 22 March 2021
Accepted Date: 31 October 2021

Please cite this article as: Lindeman, I., Hansen, M., Scholz, D., Breitenbach, S.F.M., Hartland, A., Effects of organic matter complexation on partitioning of transition metals into calcite: Cave-analogue crystal growth experiments, *Geochimica et Cosmochimica Acta* (2021), doi: https://doi.org/10.1016/j.gca.2021.10.032

Effects of organic matter complexation on partitioning of transition metals into calcite: Cave-analogue crystal growth experiments

Lindeman, I.[a], Hansen, M.[b], Scholz, D.[b], Breitenbach, S.F.M.[c], Hartland, A.[a,*]

[a]Environmental Research Institute, School of Science, Faculty of Science and Engineering, University of Waikato, Kirikiriroa (Hamilton), Waikato, New Zealand

[b]Institute for Geosciences, Johannes Gutenberg University Mainz, J.-J.-Becher-Weg 21, D-55128, Mainz, Germany

[c]Department of Geography and Environmental Sciences, Northumbria University, Newcastle upon Tyne, NE1 8ST, UK

*Corresponding author: adam.hartland@waikato.ac.nz

1. ABSTRACT

We highlight the potential for first row transition metals to carry paleohydrological signals in speleothems, and argue that these metals constitute valuable proxies for climate reconstructions. Metal availability to speleothems is hypothesised to be restricted by organic complexation, which strongly limits the free ion activity of transition metals (Co^{2+}, Ni^{2+} and Cu^{2+}) in dripwater, thereby creating a kinetic overprint on metal concentrations and isotope ratios in speleothem calcite.

This study presents the results of the first cave-analogue experiments of transition metal partitioning into calcite in the absence and presence of organic ligands. The Geological Microclimate (GeoMic) system establishes homeostatic control of air temperature and atmospheric pCO_2 (set to 20 ± 0.1 °C and 1000 ± 10 ppm, respectively), and regulates relative humidity to cave-analogue levels (>90%). Calcite was precipitated from flowing aqueous films on inclined glass plates to assess the effect of prior calcite precipitation (PCP) on metal partitioning. We report speleothem-specific inorganic K_d values for Co, Ni and Cu of ~4, 1, and 44, respectively. Pronounced PCP effects were observed in Co and Cu in the inorganic experiments, leading to strong reduction in Cu/Ca and Co/Ca, whereas Ni/Ca molar ratios remained constant.

Introduction of the organic chelating ligand nitrilotriacetic acid (NTA) overturned the behaviour of all three metals, leading to stable solution Cu/Ca ratios and progressive enrichment of Co/Ca and Ni/Ca ratios as PCP progressed and apparent K_d values <1 for all three metals. This result is confirmed in a Cu-fulvic acid experiment. We show that in the presence of organic ligands with stability constants close to those observed in natural

systems, the partitioning of transition metals into calcite is dependent on the fluid residence time and the stability of the metal-ligand complexes. Therefore, drip rate should be the first-order control on transition metal concentrations in stalagmites: opening the way to a novel and potentially quantitative paleohydrological proxy.

Keywords: Cave analogue laboratory experiments, ligands, transition metals, organic complexation, speleothem

1 INTRODUCTION

Speleothems are fundamental terrestrial archives for paleoclimate reconstruction (Blyth et al., 2016; Casteel and Banner, 2015; Dreybrodt and Scholz, 2011; Fairchild and Baker, 2012; Fairchild and McMillan, 2007; Fairchild and Treble, 2009; Moreno et al., 2010). Their wide geographical coverage and precise geochronological control (Cheng et al., 2013; Hoffmann et al., 2007) has prompted extensive research into a wide range of paleoenvironmental proxies (Fairchild and Baker, 2012). To date, a significant number of proxies have been identified and are used for climate reconstructions including stable oxygen and carbon isotopes –known to respond to variations in rainfall and temperature (Lachniet, 2009), fluorescence –indicative of the quality and quantity of organic matter present in dripwaters (Pearson et al., 2020) and speleothem minerology and petrography, for example fabric defects and nano-crystal aggregation (Frisia et al., 2000; Frisia et al., 2018). Trace element proxies in speleothem carbonate have also garnered attention, as their concentrations and stable isotope ratios (Pogge von Strandmann et al., 2017) have been shown to react sensitively to a variety of soil and karst system processes in response to variations in environmental variables (Fairchild and Baker, 2012; Fairchild et al., 2000; Fairchild and McMillan, 2007; Fairchild and Treble, 2009).

Trace element incorporation into speleothem calcite is typically described by the partition coefficient, K_d. The partition coefficient may be used to relate the trace element content of a mineral phase to that of the solution from which the mineral precipitates and is frequently normalised to the concentration of the 'carrier' element (Ca in case of speleothems) (Equation 1):

$$K_d = \frac{\left(\frac{x}{Ca}\right)_s}{\left(\frac{x}{Ca}\right)_{aq}} \quad (1)$$

where x is the trace element of interest, $_s$ indicates the solid calcite phase and $_{aq}$ outlines the aqueous (dissolved calcite) phase. Thus, a K_d value >1 indicates preferential incorporation of the trace element over calcium, while a K_d value <1 indicates that calcium is preferably incorporated into $CaCO_3$ (Fairchild et al., 2000; Fairchild and Treble, 2009; Gascoyne, 1983; Rimstidt et al., 1998; Tremaine and Froelich, 2013).

The range of trace elements used routinely as speleothem-based proxies is currently limited almost exclusively to metals which exhibit simple partitioning and for which $K_d << 1$, namely the alkaline earth metals Sr and Mg, as the role of these elements in the karst system is comparatively well-constrained (Fairchild et al., 2000; Huang and Fairchild, 2001; Tremaine and Froelich, 2013). Alkaline earth metals have proven particularly useful as indicators of past aridity, as a shift to higher X/Ca occurs with prior calcite precipitation (PCP) due to aquifer drying (Fairchild and Baker, 2012; Owen et al., 2016; Magiera et al., 2019), with the caveat that the final Sr/Ca values of speleothems is sensitive to the initial dripwater Sr/Ca and Mg/Ca values (Wassenburg et al., 2020).

Unlike the alkaline earth metals, the first-row transition metals have garnered less attention for speleothem paleoclimate reconstructions. It is known that the partitioning behaviour of metals that act as intermediate or soft Lewis acids, for example Cd, Zn, Co, Ni and Cu (Lewis, 1923), differs considerably from that exhibited by the hard Lewis acids Sr and Mg, with theoretical predictions indicating K_d >1 for these metals (Wang and Xu, 2001; Fairchild and Baker, 2012). However, the non-thermodynamic nature of partition coefficients during

calcite precipitation in most natural contexts requires partitioning behaviour under speleothem-specific conditions to be established (Morse and Bender, 1990). For instance, despite theoretical partition coefficients being greater than 1 for transition metals, apparent partition coefficients ($K_{d\ app}$) observed for actual speleothem samples are frequently <1 due to the dependence of $K_{d\ app}$ on a number of factors including calcite precipitation rate, crystal morphology, and, perhaps most importantly, complexation reactions between organic matter (OM) and trace metal ions (Fairchild and Hartland, 2010).

Organic matter serves to mobilise (Hartland et al., 2012) and stabilise first-row transition metals in dripwater (Hartland et al., 2011), to the extent that their free ion activity is many times lower than their total concentration (Hartland and Zitoun, 2018). Because of this stabilising effect of organic matter, the $K_{d\ app}$ values of transition metals are typically much lower than theoretical (inorganic) values (Fairchild and Hartland, 2010; Hartland et al., 2014), that do not account for organic complexation.

Co, Ni and Cu may be particularly sensitive candidates for hydroclimate proxies as all three form stable complexes with organic ligands (Manceau and Matynia, 2010; Zhang et al., 2013) and are sufficiently abundant to be readily discriminated from (more labile) inorganic complexes (Hartland et al., 2011; Hartland and Zitoun, 2018; Zhang and Davison, 2001). Their use for paleohydrological reconstructions in particular shows promise because of kinetic effects that arise due to organic complexation (Hartland and Zitoun, 2018). These organic complexation effects are likely to significantly alter both their availability for incorporation into calcite (Irving and Williams, 1948) and their isotope fractionation (Ryan et al., 2014; Schott et al., 2014). Cu in particular forms highly stable complexes with organic

ligands due to the Jahn-Teller effect (Jahn and Teller, 1937) and thus is of particular interest in this study.

It has previously been demonstrated that laboratory-based experiments can provide important information on trace element partitioning into calcite (Day and Henderson, 2013; Huang and Fairchild, 2001). Laboratory-based cave-analogue experiments are particularly useful as they closely model the unique cave environment and the modes of natural speleothem formation under controlled conditions. Several laboratory-based studies have derived partition coefficients for trace elements under cave-analogue conditions. For instance, partition coefficients for Mg and Sr (Day and Henderson, 2013; Huang and Fairchild, 2001), Li, Na, Co, Cd, Ba and U (Day and Henderson, 2013), and SO_4 (Wynn et al., 2018) have all been established for speleothem-like conditions in laboratory-based experiments, providing useful K_d values for comparison with real world cave systems. As yet, no extensive laboratory-based study on the incorporation of most divalent first-row transition metals into speleothem-like calcite has been undertaken.

The purpose of this study is twofold: First, we address the need for representative inorganic K_d values for Co, Ni and Cu under precisely controlled speleothem-specific conditions in the absence of organics. In a second set of experiments, by adding known organic components to the solution, we assess the effect of organic complexation of Co, Ni, and Cu partitioning into speleothem-like calcite, to aid the interpretation of Co, Ni and Cu signals in speleothem samples as environmental proxies. The comparison of these approaches provides important new constraints on the likely drivers of Co, Ni and Cu in speleothems.

2 METHODS AND MATERIALS

2.1 Overview

Four calcite crystal growth experiments were carried out under cave-analogue conditions in order to meet the aims of this study (Table 1). Two replicated inorganic crystal growth experiments (experiments 1 and 2) were undertaken initially to provide speleothem-specific K_d values for Co, Ni and Cu. Subsequently, two experiments were carried out with organic ligands nitrilotriacetic acid (NTA, experiment 3) and Suwannee River Fulvic Acid (SRFA, experiment 4) present to determine the degree to which Natural Organic Matter (NOM) complexation affects the partitioning of these metals.

2.2 GeoMic: The Cave-Analogue System

All four crystal growth experiments were undertaken inside a purpose-built climate-controlled chamber based closely on the design developed by Hansen et al. (2017; 2019). This system, hereafter referred to as GeoMic (Geological Microclimate), is an in-house built state-of-the-art climate-control box with a chamber of well-defined atmosphere and precisely controlled temperature, humidity and CO_2 concentration. GeoMic was equipped with a four-channel high-precision Hei-FLOW peristaltic pump (Heidolph Instruments GmbH & Co., Schwabach, Germany) to precisely control drip rate and volume, a HUMICAP HMP7 relative humidity and temperature probe (Vaisala Oyj; Vantaa, Finland), and a CARBOCAP GMP252 carbon dioxide probe (Vaisala Oyj; Vantaa, Finland). The temperature inside GeoMic was controlled via a recirculating chiller module (PolyScience, model number NO772025; Niles, IL, USA) coupled to a radiator fan inside the enclosure and monitored via three NTC thermistors. Atmospheric pCO_2 was controlled via the addition of N_2 and CO_2 gases through computer-controlled magnetic valves as required. A purpose-built LabVIEW software program installed on GeoMic's computer allowed automatic control of the

recirculating chiller and the magnetic valves to adjust temperature and pCO_2 within the chamber via feedback from the Vaisala probes. Humidity was kept as high as possible throughout the experiments by continuously bubbling the atmosphere (and introduced gases) through deionised water. Atmospheric data were logged by the LabVIEW software for the duration of the experiments at one-minute intervals.

Manual manipulation of an experiment after the chamber had been sealed to the outside environment was achieved through four nitrile isolator-box gloves installed on the front face of the GeoMic chamber. A sample port at the end of the chamber allowed samples to be removed during the experiment with minimal gas, temperature and humidity exchange between in-box and outside environment. A photo of the GeoMic system is provided in Fig. 1.

The control of environmental parameters, presented in Fig. 2, was generally very precise, with the exception of relative humidity (RH) in the latter stages of experiments 1 and 4 (Fig. 2c). The GeoMic system provided highly stable conditions that enabled us to constrain the influence of temperature (Fig. 2b), humidity (Fig. 2c) and CO_2 (Fig. 2a) on the partitioning behaviour of Co, Ni and Cu into calcite. CO_2 pressure remained within ±1% of the set point for the majority of the experiments but became more variable in the final quarter of all experiments, particularly experiment 2, where values varied within ±10% of the set point (Fig. 2a).

2.3 Materials

For the experiments, we used $CuCl_2{\cdot}2H_2O$, $CoCl_2{\cdot}6H_2O$, $NiCl_2{\cdot}6H_2O$, nitrilotriacetic acid (NTA), and lycopodium powder, which were supplied by British Drug House (BDH) Limited. $CaCO_3$ and $CaCl_2$ were supplied by Sigma Aldrich. Suwannee River Fulvic Acid (SRFA) was obtained from the International Humic Substances Society. Analytical grade CO_2 and N_2 were used for all experiments (supplied by the British Oxygen Company). Both the multi-element inductively coupled plasma-mass spectrometry (ICP-MS) standard and the single element calcium standard were supplied by Inorganic Ventures (Christiansburg, VA, USA).

2.4 Solution Composition and Aqueous Speciation Modelling

To ensure calcite growth experiments analogous to calcite growth in a natural cave (i.e., closely resembling natural speleothem precipitation), a method that fostered crystal growth via CO_2 degassing was adopted (Hansen et al., 2019). To simulate a reservoir of dripwater, the method of Hansen et al. (2013) was used. In detail, 5 g of $CaCO_3$ were dissolved in 10 L of deionised water to make a solution of 5 mM $CaCO_3$, and trace elements and organic ligands were added as required for each experiment (Table 1). CO_2 gas was sparged through this solution until the reservoir became clear. The pH of the solution at this point was approximately 5 for all experiments, and the solution was undersaturated with respect to calcite (calculated with PHREEQC) (Parkhurst and Apello, 1999). In typical cave systems, where the dripwater remains in the aquifer for sufficiently long periods to reach chemical equilibrium with the host rock, the calcite saturation index (SI) of the water in the aquifer is theoretically 0 (Dreybrodt and Scholz, 2011). Thus, the undersaturated solution was sparged with N_2 gas until the solution became only slightly undersaturated with respect to calcite (SI ≈ -0.09, pH = 6.4). A SI index of exactly 0 was not used in order to avoid calcite precipitation

occurring inside the reservoir and/or tubing. Once prepared, the solution was immediately sealed to the environment, and was equilibrated to 20°C in GeoMic for 48 hours. The species distribution in the initial reservoir solutions was modelled using visual MINTEQ 3.0 speciation codes (Allison et al., 1991). Complexation with SRFA was modelled using the NICA-Donnan model in visual MINTEQ, which utilises a bimodal, continuous distribution for protons and metal ions (Kinniburgh et al., 1999).

2.4.1 Organic Ligand Characteristics

The chelating ligand NTA was chosen for experiment 3 on the basis of its high stability constants for Co-NTA (log$K$ = 10.4), Ni-NTA (log$K$ = 11.5) and Cu-NTA (log$K$ = 12.9) complexes (Giorgio, 1982; Martell and Smith, 1975; Parker et. al 1995), which are close to the conditional stability constants found by Hartland and Zitoun (2018) for Cu-NOM complexes in dripwater from four caves in Aotearoa (New Zealand) (log$K_{\text{Cu-NOM}}$ ≈ 13.5-15.5). SRFA (experiment 4) was chosen because its heterogeneity is more representative of NOM observed in karst systems (Blyth et al., 2016), and for being well-characterised in the literature (Cabaniss, 1990; Cabaniss and Shuman, 1988; Leenheer et al., 1998; Rostad and Leenheer, 2004). Ligand concentrations were selected in order to provide high levels of trace metal complexation, as observed for Co, Ni and Cu in typical dripwater (Hartland et al., 2014; Hartland and Zitoun, 2018). The concentration of NTA used in experiment 3 was also based on the molar ratio of NTA to Ni used by Zhang et al. (2013) during their kinetic studies of Ni organic complexes via diffusive gradients in thin films (DGT). Due to limitations on the amount of available SRFA, a Cu-only experiment was carried out in experiment 4. Modelling in visual MINTEQ predicted that, had Co and Ni been included, the proportion of complexed Co^{2+} and Ni^{2+} in the initial solution would have been significantly lower than 100%, making comparison with the NTA experimental results difficult.

Visual MINTEQ aqueous speciation modelling of initial solution compositions (Table 2) indicated that Cu, Ni and Co in the inorganic system (experiments 1 and 2) were present primarily as aquo-M^{2+} species, or in simple inorganic complexes expected to be characterised by fast dissociation rates. In contrast, for experiment 3, modelled results showed M-NTA^- species constituted 90%, 99% and 99.8% of species for Co, Ni and Cu, respectively. Cu-SRFA complexes accounted for 96% of the Cu species in experiment 4.

2.5 Experimental Design

After the reservoir had reached the experimental temperature, and pCO_2, humidity, and temperature in the GeoMic chamber had stabilised, the solution was dripped via the peristaltic pump onto a 190 cm long, 3°-tilted glass plate with two 4 cm-wide 'channels' defined at the edges by adhesive tape. A sandblasted glass plate was used to provide calcite nucleation sites and a stable flowing solution film. A thin solution film was established in both channels, and the characteristics (e.g. residence time, flow velocity, film thickness) of both thin films were assessed (the relevant characteristics and methods are analogous to Hansen et al. (2019) and are provided in the Supplementary Information Section S2 and Table S1). Degassing of dissolved CO_2 occurred in all experiments during the first *ca*. 4 cm, documented by the rise in pH to values of *ca*. 8. Thus, the solution became supersaturated with respect to calcite, as demonstrated by Hansen et al. (2013). As the thin solution film flowed down the plate, $CaCO_3$ was progressively precipitated along the flow path. At the end of the plate, the solution dripped into the sampling port, where it drained to waste. This precipitation process was allowed to continue uninterrupted for 72 hours. $CaCO_3$ precipitation rates were calculated from electrical conductivity measurements following the method of Hansen et al. (2013; 2019), see Supplementary Table S2.

The two-channel design of these experiments sets them apart from previous laboratory-based trace element partitioning studies by allowing characterisation of both the precipitated $CaCO_3$ and dripwater solutions simultaneously. Comparison of the directly precipitated carbonate on the glass plates with the solution samples enables calculation of K_d values at different stages of the experiment (i.e., after specific amounts of PCP) (Hansen et al. 2019). After 72 hours, flow to one of the channels (referred to as the reference channel) was interrupted, so that calcite precipitated in this channel could be sampled at different distances (residence times) in order to determine trace element content. Flow continued through the other channel (referred to as the sampling channel) and water samples were collected at different residence times in order to determine the trace element and organic matter content of the 'dripwater'. The distance of flow was adjusted by shifting the drip site down the plate, and at each new distance the thin film was left to equilibrate for 30 min before sampling. Water samples for Inductively Coupled Plasma Mass Spectrometry (ICP-MS) measurements (7 mL), pH measurements (5 mL) and electrical conductivity measurements (EC, 10 mL) were collected in 15 mL polyethylene terephthalate (PET) centrifuge tubes for each distance within the sealed sample port. A schematic of the experimental set up is provided in Fig. 3.

2.6 Analytical Methods

2.6.1 Inductively Coupled Plasma Mass Spectrometry

Solution samples were acidified with doubly distilled concentrated HNO_3 (Savillex DST-1000 Acid Purification System; Eden Prairie, MN, USA) to 2% (v/v) prior to analysis. Of precipitated samples, ~ 2 mg of $CaCO_3$ were removed from the reference channel plate at each distance of flow and dissolved in HNO_3 (5%, 8 mL). Acid blanks of 2% doubly distilled HNO_3 (v/v) were included in each run.

Elemental analysis was performed at the University of Waikato using an Agilent 8900 ICP-MS, controlled by MassHunter Workstation Version 4.5 and connected to an SPS4 autosampler. A 0.05-0.1 mL min^{-1} micromist U-Series nebuliser was attached to a quartz cyclonic spray chamber followed by a quartz torch with a 2.0 mm injector. Nickel sampler and skimmer cones followed the plasma torch, and an omega lens was used for ion beam focussing. The ICP-MS instrument was optimized to maximum sensitivity before each run, to ensure oxides and doubly-charged ions were fewer than 2%.

Five-point calibration curves for Co, Ni and Cu were constructed using a multi-element standard with concentrations ranging between 0.1 and 500 ppb, while the five-point calibration curve for Ca was based on concentrations between 100 and 10,000 ppb. A single-element standard was used for the Ca calibration curves. Re-calibration was undertaken after every 100 samples, check-standards were analysed after each batch of 20 samples and used for drift correction, and blank samples were analysed after every 10-sample batch to reduce sample carry-over. Sc was used as the internal standard for Ca analysis, while Y was used as the internal standard for Co, Ni and Cu. Samples were analysed in triplicate to assess analytical error. Isotopes used for quantification were ^{43}Ca, ^{59}Co, ^{60}Ni and ^{65}Cu for all experiments except experiment 4 (SRFA), where ^{44}Ca was used due to matrix interferences with ^{43}Ca.

2.6.2 Fourier Transform Infra-Red (FTIR) Spectroscopy

The precipitates from between 20 and 25 cm on the sampling channel of each experiment were taken for structural characterisation. Sub-samples were mixed and homogenised with oven-dried (100°C) KBr at an approximate ratio of 1:50 in an agate mortar and pestle, before

being compressed into discs under 10,000 kg of pressure. Spectra were collected on a Perkin-Elmer Spectrum 100 spectrometer at a resolution of 1 cm^{-1} with eight scans ranging between 600–1200 cm^{-1}, following the method developed by Ni and Ratner (2008). Background measurements of a blank KBr disc were taken and subtracted from the sample spectra using the software package Spectrum (version 6.3) default method.

2.6.3 Powder X-ray diffraction (pXRD)

$CaCO_3$ crystals precipitated during each experiment were characterised on a Panalytical Empyrean XRD. The XRD patterns were collected at a scanning rate of 0.02 ° s^{-1} in 2θ with diffraction angles from 20 θ to 60 θ. A Cu Kα radiation energy of 40 kV and 20 mA was used, following the procedure outlined by Ni and Ratner (2008).

2.6.4 Scanning Electron Microscopy (SEM)

Scanning electron microscopy was undertaken to characterise the microstructures of the crystals precipitated from each experiment, using a Hitachi S-4700 cold field emission microscope. Samples were sputter coated in an ultra-thin layer of platinum and palladium for sample conductivity. After coating, the $CaCO_3$ crystals were taped to aluminium stubs and observed in scanning mode using a voltage of 5 kV.

2.6.5 Fluorescence Analysis of Growth Solutions and Calcite Samples

In order to determine the extent of SRFA ligand incorporation into the $CaCO_3$ during experiment 4, both solution and precipitate samples were measured for 3D excitation emission matrix (3D EEM) fluorescence using a Horiba Jobin Yvon Aqualog spectrometer with a CCD detector. Measurements were taken in the excitation emission range of 240-600 and 245-800 nm, with 0.5 sec integration time and at 3 nm step-size (Pearson et al., 2020).

Each matrix was corrected for inner-filter effects, scatter lines were Rayleigh masked (both first and second order), and spectra were normalised to the average Raman intensity of deionised water using Aqualog's data processing software (Gilmore and Cohen, 2013).

To ensure complete dissolution of organic matter and $CaCO_3$, solution samples were acidified to 0.025 M HCl prior to 3D EEM analysis. Precipitates (2 mg) were dissolved in dilute HCl (0.025 M, 4 mL) following the method outlined by Pearson et al. (2020). A five-point calibration curve for SRFA was constructed with concentrations ranging between 1 and 20 ppb. Standards were acidified to 0.025 M HCl and matrix matched to the solution samples via addition of $CaCl_2$ to the same ionic strength as that of the reservoir solution (I=0.02). Blank samples were analysed after every 10-sample batch.

The 3D EEM data were processed with MATLAB using parallel factor analysis (PARAFAC) as implemented in the N-way toolbox (Andersson and Bro, 2000), and the drEEM toolbox (Murphy et al., 2013). PARAFAC provides multi-way data analysis in which the underlying phenomena of fluorescence can be distinguished and separated into statistically valid components (Fellman et al., 2010; Ishii and Boyer, 2012). A one-component PARAFAC model was used for all samples, as only one meaningful fluorescence (humic-like) component was produced. The fluorescence spectra of the SRFA solutions (Fig. 4) were dominated by the humic-like fluorescence peak 'A' (ex 250-260 nm; em 380-480 nm) (Coble, 1996). This peak has been well documented in humic material from terrestrial environments including cave systems (Coble, 1996; Hartland et al., 2010; Rutlidge et al., 2014). The calibration curve between PARAFAC C1 scores and SRFA concentration used to calculate [SRFA] in experiment 4 is presented in Fig. 4.

3 RESULTS AND DISCUSSION

3.1 Structural Characterisation of $CaCO_3$ precipitates

FT-IR spectra (Fig. 5) of the precipitated $CaCO_3$ in each experiment show the characteristic v_4 and v_2 bands of calcite at 713 cm^{-1} and 874 cm^{-1} (Fig. 5a), respectively, and were consistent with reported spectra for pure calcite crystals (Ni and Ratner, 2008; Pearson et al., 2020). Spectra for experiments 1-3, however, also show the characteristic v_4 band of vaterite at 744 cm^{-1} and a band at ~1090 cm^{-1} (mode unknown, Fig. 5a) that has also been reported to be related to vaterite by Ni and Ratner (2008). These bands were not observed for $CaCO_3$ precipitated during experiment 4. Characteristic bands for aragonite (v_2 at 858 cm^{-1} and v_4 at 700 cm^{-1}) were absent from all spectra (Ni and Ratner, 2008). To ensure the polymorph remained consistent along the flow path during each experiment, samples from three different distances along the plate were analysed, but for clarity, only one spectrum for each experiment is included in Fig. 5. Results indicate that the polymorphs of $CaCO_3$ along the plate are consistent in each experiment.

pXRD was also carried out on precipitates from experiments 1-3, while insufficient $CaCO_3$ precipitated during experiment 4 for this analysis. The obtained pXRD patterns were consistent with the FT-IR results (Fig. 5) and indicate a mixture of calcite and vaterite. We found all major peaks reported in the literature for calcite, while some minor peaks, indicative of vaterite, were also seen at 2θ diffraction angles 55, 50, 33 and 25 (Fig. 5b) (Ni and Ratner, 2008).

SEM micrographs (Fig. 6) were taken of precipitates from experiments 1-4 to provide information on crystal morphology. The majority of crystals display rhombohedral morphology in all experiments, consistent with calcite (Pearson et al., 2020). Overgrowth, aggregation of crystals, and growth defects were observed to varying degrees in all experiments, with the highest proportion of defects found in experiment 4. As expected, a minority of crystals with morphologies typical of vaterite were found in experiments 1-3 (Hu et al., 2012).

The presence of small quantities of vaterite in precipitates from experiments 1-3, and the absence of vaterite in experiment 4 indicate polymorph variability caused by relatively high total trace metal concentrations. Earlier work (Meldrum and Hyde, 2001; Zhang and Dawe, 2000) suggested that trace metal concentrations may cause changes in $CaCO_3$ crystal morphology and polymorph (formation of aragonite at high trace metals concentrations has been well documented). Thus, it is likely that the higher concentrations of trace metals in experiments 1-3 ($[M]_{total}$ = 150 ppb) caused formation of vaterite. In experiment 4, only rhombohedral calcite was precipitated, presumably due to lower total trace metal concentrations ($[M]_{total}$ = 50 ppb). Because vaterite was only a minor contributor to the $CaCO_3$ formed in these experiments, our results are considered to be representative of speleothem $CaCO_3$ deposits. Furthermore, although calcite is the primary $CaCO_3$ polymorph in speleothems, Frisia et al. (2018) suggested that vaterite crystals are likely one of the many possible initial or 'precursor' states of speleothem crystallization.

The presence of organic material in solution was found to cause morphological changes in calcite crystals. Crystals formed under inorganic conditions displayed clear rhombohedral morphology with defined edges and corners and well-developed flat faces (Figs. 6A-6F). In

contrast, calcite crystals grown in the presence of 2 ppm NTA displayed rounded corners and a high density of steps and sub-micron scale kinks on the crystal faces (Figs. 6G-6I). These features are pronounced in calcite precipitated in the presence of 20 ppm SRFA (see SEM micrographs in Figs. 6J-6L), and previous work has identified that these features are characteristic of calcite grown in the presence of organic matter (Frisia et al., 2018; Pearson et al., 2020).

3.2 Transition Metal Partitioning Under Inorganic Conditions

Previously published partition coefficients for the first-row transition metals Co, Ni and Cu into calcite do not represent partitioning under speleothem-like conditions and are of limited value to the speleothem science community (Kitano et al., 1973; Kitano et al., 1980; Lorens, 1981; Rimstidt et al., 1998). In the first phase of this study, we experimentally derived representative inorganic K_d values for Co, Ni and Cu under precisely controlled cave-analogue and speleothem-specific conditions.

3.2.1 Derivation of inorganic K_d values

The partitioning of Co, Ni and Cu into $CaCO_{3(s)}$ was assessed for multiple residence times along the plate in experiments 1 and 2. For each residence time on the plate, trace metal and Ca concentrations in solution and precipitate samples were determined by ICP-MS. We used Equation 1 to calculate K_d values for each element at each residence time, and to calculate a K_d value for the entire plate for each element (Table 3). No Cu data is available for experiment 2 as [Cu] fell below the quantification limit (QL) of the ICP-MS method for solution samples taken at all residence times. This likely resulted from a small amount of

$CaCO_3$ precipitation occurring in the solution reservoir and tubing prior to sampling: the high partition coefficient of Cu ensuring its incorporation into this precipitate and possible adsorption of Cu to this precipitate. This interpretation is supported by an observed 4.2 % reduction in [Ca] between the reservoir and drip site observed for experiment 2 that was not observed for experiment 1, and a visual inspection showing a solid white precipitate in the tubes prior to the dripsite. Although Cu was measurable in three of the solution samples taken from experiment 1, its high partition coefficient again resulted in [Cu] falling below the QL after a residence time of 42 s as it was readily incorporated into the precipitated calcite. This is consistent with the high K_d values reported for Cu in the literature (Wang and Xu, 2001).

In order to determine whether the M/Ca ratios could be predicted based on known partition coefficients, we modelled expected M/Ca ratios as PCP progressed using Equation 1. For this exercise, we used both the experimental whole plate K_d values determined in this study (presented in Table 3) and theoretical partition coefficients reported by Wang and Xu (2001). Figs. 7 and 8 show the modelling results alongside experimental M/Ca ratios as determined for experiments 1 and 2, plotted against fractional PCP.

Data was plotted as a function of calcite precipitation in order to show the possible effects expected after varying levels of PCP in a natural system. Fractional PCP was calculated as follows:

$$1 - \frac{[Ca]_d}{[Ca]_i} \qquad (2)$$

where $[Ca]_d$ is the dissolved concentration of calcium at distance d and $[Ca]_i$ is the initial concentration of calcium in dripwater.

3.2.2 Inorganic K_d values for Co, Ni and Cu

High inorganic K_d values were found for Co (whole plate K_d values = 4.4 ± 0.3 and 3.6 ± 0.5 for experiments 1 and 2, respectively), indicating Co^{2+} was preferentially incorporated over Ca^{2+} into the calcite lattice at all levels of PCP. Figs. 7e and 8a shows $Co/Ca_{(aq)}$ decreased along the plate as PCP progressed, as predicted by the model based on the experimentally determined whole plate partition coefficient. Trends in $Co/Ca_{(s)}$ varied between experiments 1 (Fig. 7f) and 2 (Fig. 8b), with experimental data fluctuating around the model-predicted values. In contrast, the inorganic K_d values found for Ni (whole plate K_d values = 1.1 ± 0.1 and 0.7 ± 0.01 for experiments 1 and 2, respectively) demonstrated that Ni^{2+} partitions into calcite at a rate similar to Ca^{2+}. This resulted in $Ni/Ca_{(aq)}$ remaining virtually constant at all levels of PCP (Figs. 7c and 8c). $Ni/Ca_{(s)}$ however did not remain constant as PCP progressed (Figs. 7d and 8d), thus deviating from the model. Possible reasons for fluctuations in $Ni/Ca_{(s)}$ and $Co/Ca_{(s)}$ not predicted by the model will be discussed in Section 3.2.3.

The evolution of Cu/Ca during experiment 1 differed markedly from the evolution of both Ni/Ca and Co/Ca (Fig. 7). The very high affinity of Cu^{2+} for the calcite lattice (whole plate K_d = 44 ± 3) caused $Cu/Ca_{(aq)}$ to initially drop steeply, with concentrations of Cu in solution samples quickly falling below the ICP-MS QL (Fig. 7a). $Cu/Ca_{(s)}$ also dropped steeply as Cu was rapidly lost from solution in the first half of the plate.

Unsurprisingly, K_d values for each element changed with progressive PCP (although this change was minimal for Ni) as a result of the system being driven out of equilibrium by progressive precipitation of $CaCO_3$. Therefore, although whole plate K_d values are presented

here, the partitioning of uncomplexed Co, Ni and Cu may be better described by the K_d values determined for the shortest residence times (i.e., first few cm of flow), as these are likely to be closer to the "true" equilibrium partition coefficients. This is particularly relevant for stalagmites with short dripwater residence times (Mühlinghaus et al. 2009)

Alternatively, the effects of changing $CaCO_3$ precipitation rate may also have influenced the evolution of K_d values as PCP progressed. It has previously been shown that precipitation rate can be a significant factor influencing the trace metal content of naturally occurring calcite, with the general consensus being that K_d values < 1 decrease with decreasing precipitation rate while those > 1 increase with decreasing precipitation rate (Lorens, 1981; Morse and Bender, 1990; Ohara and Reid, 1973; Tesoriero and Pankow, 1996). It may then be expected that as the precipitation rates decreased along the plate (see Supplementary Table S2), K_d values for Co and Cu should have increased accordingly. Indeed, a general increase was observed for both Co and Cu (Table 3). However, other authors have observed that over the range of growth rates observed in natural speleothems (similar those observed here) the influence of growth rate on partition coefficients may be negligible and the fraction of calcium remaining in solution (dictated by the extent of PCP) is likely the dominant control on trace element ratios (Day and Henderson, 2013). With the exception of Ni (Lakshtanov & Stipp, 2007), the lack of information pertaining to the effects of $CaCO_3$ precipitation rate on the partition coefficients of transition metals over the range of growth rates observed during these experiments means we cannot rule out that changes in growth rate as PCP progressed influenced the resulting K_d values observed.

3.2.3 Inorganic Modelling Results

$Co/Ca_{(aq)}$ and $Ni/Ca_{(aq)}$ ratios in solution samples observed in both inorganic experiments 1 and 2 are in good agreement with predicted values (based on Equation 1) and the experimentally determined (static) partition coefficients (Table 3). The models employing the theoretical K_d values of Wang and Xu (2001) on the other hand predicted a significant decrease in $Co/Ca_{(aq)}$ and $Ni/Ca_{(aq)}$ as calcite precipitation progressed, suggesting that for speleothem-specific conditions, the theoretically predicted K_d values for Co and Ni are too high. By comparison, the deviation between experimental and modelled $Co/Ca_{(s)}$ and $Ni/Ca_{(s)}$ ratios was small for models based on our experimentally determined K_d values.

These discrepancies between predicted and experimental Co/Ca and Ni/Ca values are likely due to three factors. Firstly, as precipitation occurs along the plate, the system moves away from equilibrium, causing a change in K_d values for each element as PCP progresses. Secondly, changing precipitation rate along the plate is also likely to have influenced K_d values to some degree, particularly for Co. Finally, it is probable that competition for Ca^{2+} lattice sites between different metals caused unexpected deviations from predicted values. This interpretation is supported by increasing $Co/Ca_{(s)}$ and $Ni/Ca_{(s)}$ ratios in the precipitates after [Cu] in the solution fell by 98% in experiment 1. Fig. S17 illustrates the development of total metal concentrations [M] in the experiment 1 precipitate with progressing PCP. After ~20% PCP, $[M]/Ca_{(s)}$ is already significantly reduced due to Cu loss from the solution, and we suggest that at this point $[Co]_{(s)}$ and $[Ni]_{(s)}$ increased as competition for lattice sites diminished. It should be noted, however, that competition for lattice sites is not likely to be important in natural systems where the concentration of metals is significantly lower than those seen here.

As mentioned above, the high affinity of Cu^{2+} for the calcite lattice caused $Cu/Ca_{(aq)}$ to drop steeply initially, with concentrations of Cu in solution samples quickly dropping below the ICP-MS QL (Fig. 7a). Although the models generally capture this decrease, they deviate from the experimental data for both precipitate and solution samples, predicting an even faster loss of Cu from solution than actually observed (Figs. 7a and 7b). Deviations from the model are again primarily attributable to changing $CaCO_3$ precipitation rate and the trend away from equilibrium conditions, which cause a change in K_d values with progressive PCP. As deviations from the predicted X/Ca values were greatest for Cu, it is likely that single static partition coefficients to describe metal partitioning into speleothem calcite are most suitable for metals with low partition coefficients (e.g., Ni).

In order to determine whether a dynamic, PCP-adjusted, K_d value could better predict the M/Ca ratios observed in solution and precipitate samples, we regressed the K_d values for each element against PCP and used the resulting equations to calculate K_d values for each distance step in the model (see Supplementary Information S3 for details). However, this modelling exercise did not provide a more accurate prediction of X/Ca ratios in solution and precipitate samples, indicating that the effect of changing solution composition on partitioning behaviour is not a simple linear dependence of K_d values on extent of PCP. This is an understandable outcome as the effects of competition for lattice sites and changing precipitation rate are unlikely to be accounted for by a simple linear relationship.

3.2.3 Comparison of Inorganic K_d *Values with Previously Published Values*

The various analytical methods, experimental conditions, solution composition and modes of calcite precipitation employed by previous researchers complicate a direct comparison between our experimental K_d values and previous results (see Table 5). Most published

values do not represent partitioning under speleothem-like conditions (Kitano et al., 1973; Kitano et al., 1980; Lorens, 1981; Rimstidt et al., 1998) and are thus expected to differ to the results reported here. However, comparison of published and newly derived partition coefficients indicates a consistent general order of magnitude for the K_d values of Co, Ni and Cu. For example, Wang and Xu (2001) developed a linear free energy correlation model to predict partition coefficients based solely on the chemical bonding energies of cations within a host mineral and the excess energy resulting from size differences between the host cations and the substituting trace ion. They predicted partition coefficients for Co, Ni and Cu partitioning into calcite of 9.33, 3.47 and 37.15, respectively, indicating that Cu would incorporate more readily into calcite then Co, and then Ni. The speleothem-specific partition coefficients found here are evidently consistent with this prediction.

The partition coefficient reported by Day and Henderson (2013) for Co is of more relevance due the cave-analogue nature of their experiments. The partition coefficient was calculated to be 1.87 at a temperature of 20°C. Although the partition coefficients derived here for the whole plate in experiments 1 and 2 were higher (4.4 and 3.6, respectively), comparable K_d values of 1.80 ± 0.3 and 1.97 ± 0.1 were observed in experiment 2 at early stages with 0 % and 10.5 % PCP, respectively.

For Ni, the whole plate K_d value determined in experiment 1 is consistent with that proposed by Lakshtanov and Stipp (2007), who found that for dilute solid solutions, Ni partition coefficients were *ca.* 1. A K_d value of 1 is of significance because, as was found by Lakshtanov and Stipp (2007), calcite precipitation rate should not significantly affect the partitioning behaviour of Ni. Indeed, our results indicate that Ni may be a valuable speleothem-based driprate proxy (see Section 3.4) because its ratio to calcium is largely

independent of PCP. Hence, Ni/Ca changes in speleothems should be independent of Sr, Ba and Mg in the many instances where the behaviour of the alkali earth metals is dominated by PCP.

3.3 Transition Metal Partitioning Under Organic Conditions

Having studied the behaviour of transition metals under speleothem-specific, inorganic conditions, we then evaluated the effect of organic ligands on their partitioning behaviour, thereby approaching real-world conditions.

To assess the impact of OM complexation on partitioning of Co, Ni and Cu into calcite, M/Ca ratios in solution and precipitated calcite were determined for experiments 3 and 4. K_d values for each element at different distances of flow and the K_d values for the entire plate for each element are summarised in Table 4. It is evident that the presence of organic ligands in solution mediated the partitioning of all three metals into calcite, with significantly lower amounts of all three metals incorporated into the $CaCO_3$, overall. K_d values for each metal were significantly lower in experiments 3 and 4 compared to the inorganic experiments 1 and 2, indicating that complexation by OM reduced the availability of 'free' metal ions for incorporation into the calcite lattice. These partition coefficients are significantly closer to those observed by Hartland et al. (2014) in real cave systems. It should be noted that although a significant decrease in partition coefficients was observed, the order of partition coefficients determined for the inorganic experiments (Cu > Co > Ni) was preserved. Figs. 9 and 10 show M/Ca ratios in solution and precipitate as PCP progressed in experiments 3 and 4, respectively. No $Cu/Ca_{(s)}$ data is presented for calcite precipitated in experiment 4 as low growth rates caused by high concentrations of OM (as observed previously by Pearson et al., 2020) led to an insufficient amount of $CaCO_3$ for sampling at most distances of flow.

Modelling of expected M/Ca ratios as calcite precipitation progressed was also undertaken for experiments 3 and 4 (results presented in Figs. 9 and 10). To do so, we calculated the concentration of complexed metal for a range of residence times according to the first order rate law (Amery et al., 2010):

$$[ML] = [ML]_i e^{-kt} \quad (3)$$

where [ML] is the concentration of complexed metal at time t, $[ML]_i$ is the initial concentration of complexed metal and k is the dissociation rate constant. This allowed the calculation of the amount of 'free' (i.e. uncomplexed) metal, f_m, at different residence times. To calculate the amount of dissociated metal (f_m) at each theoretical 'step' of fractional PCP in the models, we correlated residence times to PCP via a linear regression for each experiment. Subsequently, the partitioning of f_m (first determined by equation 3) as PCP occurred was modelled using Equation 1, and the experimental inorganic whole plate K_d values determined in experiment 1. The first order dissociation rate constant used for modelling Ni dissociation from NTA (2×10^{-4} s^{-1}) was taken from Zhang et al. (2013). Because we could not find any dissociation constants for CoNTA or CuNTA complexes in the literature, we used dissociation constants for these metals that produced the model with the best fit to the data (9.5×10^{-4} s^{-1} and 1.4×10^{-3} s^{-1} for Co and Cu, respectively). Although these rate constants need to be verified, they provide a reasonable estimate of dissociation rate constants for the desired purpose (and respect the known hierarchy of NOM dissociation rates among these metals (Warnken et al., 2007; Zhang and Davison, 2001)). The rate constant used for modelling the dissociation of CuSRFA complexes was 3.1×10^{-3} s^{-1}, based

on the constant found by Chakraborty et al. (2014) for dissociation of Cu complexes with Suwannee River Natural Organic Matter (SRNOM).

3.3.1 Transition metal partitioning in the presence of NTA

Experimental partition coefficients calculated for Co, Ni and Cu in experiment 3 (Table 4) were significantly lower than those observed during the inorganic experiments. Whole plate K_d values of ~0.4, ~0.03 and ~0.9 for Co, Ni and Cu support the argument that binding by OM can significantly impact the partitioning behaviour of the first row transition metals into calcite, and that the impact of complexation by OM in natural systems must be considered when interpreting signals of Co, Ni, Cu in speleothems. Indeed, this presumably extends to other transition metals and elements (e.g. REE) with known affinity for organic complexation (Tang and Johannesson, 2003).

Solution data from the NTA experiment (experiment 3) agree within error with model results (Fig. 9a). In stark contrast to the inorganic results (Figs. 7c, 7e, 8a, and 8c), we found a slow increase in $Co/Ca_{(aq)}$ and $Ni/Ca_{(aq)}$ in solution with progressing PCP. For Co and Ni, this suggests that complexation by NTA serves to stabilise Co^{2+} and Ni^{2+} in the dissolved phase, minimising their loss due to calcite precipitation. The $Cu/Ca_{(aq)}$ ratios (Fig. 9a) showed fairly consistent values along the plate with some slight variation around a mean of 0.135 mM/M. Again, this starkly contrasts to the steep decrease observed for Cu in the inorganic system (Fig. 7a) and indicates that the stabilisation of Cu^{2+} by NTA effectively balanced the Cu distribution between aqueous and solid phases. So, although Cu has a particularly high inorganic partition coefficient, the high stability of CuNTA complexes ensures Cu loss from solution at an almost constant rate.

The results for the precipitate samples from experiment 3 agree less well with the modelled values, which predicted a slow increase in $Co/Ca_{(s)}$ (Fig. 9b) and $Ni/Ca_{(s)}$ (Fig. 9b) with progressing PCP. However, the experimental data show that $Co/Ca_{(s)}$ and $Ni/Ca_{(s)}$ remained fairly consistent along the plate with small variations around mean values of 0.07 and 0.005 mM/M, respectively (Fig. 9b). A modelled decrease in $Cu/Ca_{(s)}$ was consistent with our experimental data determined for the last half of the plate. However, an initial increase in sexperimental Cu/Ca values at the start of the plate was not captured by the model (Fig. 9b).

Deviations from predicted M/Ca ratios observed in experiment 3 (Fig. 9) may be explained by two major limitations of the modelling approach. Firstly, the dissociation constants used to predict the release of metal from organic complexes were constant across the entire plate. In reality however, it is unlikely that the stability and thus dissociation rates of the complexes stayed the same as PCP progressed. This is because there would have been a reduction in the solution M:NTA ratio as the partitioning of trace metals into calcite progressed (assuming that the trace metals partitioned into calcite more readily than NTA itself). This decrease in M:NTA would cause an increase in complex stability, and thus presumably an increase in the time required for complex dissociation (Hering and Morel, 1988; Morel, 1983; Rate et al., 1993; Warnken et al., 2007).

Secondly, the effects of ternary complexation have not been accounted for in these models as the concentration of NTA in solution and precipitate samples was not assessed. Previous studies have shown that ternary complexation can play a role in trace element partitioning into speleothem calcite, particularly for highly stable complexes (Hartland et al., 2014). In order to assess whether the deviation from model predictions could realistically be a result of

ternary complexation, the large deviation between the predicted and experimental $Ni/Ca_{(s)}$ values observed at ~7 % PCP was taken as an example (experiment 3, Fig. 9b). The difference between model and experimental data could be explained if 0.18 % of the NiNTA complexes present in solution (equal to 0.07 % of the total NTA species) were partitioning into the $CaCO_3$ via ternary complexation. Previous studies have demonstrated that dissolved OM may indeed be incorporated into calcite to this degree. For instance, Hartland et al. (2014) reported a 3 % removal efficiency of organic carbon in the stalagmite PC-08-1 (Poole's Cavern, UK). Thus, ternary complexation may explain to some degree the deviations in $M/Ca_{(s)}$ for each trace metal, however this was not the case for the SRFA experiment (see Section 3.4 for more detail on ternary complexation).

3.4 Is Ternary Complexation Important for Transition Metal Partitioning?

Ternary complexation can be described as the incorporation of NOM-M complexes into $CaCO_3$ precipitates without metal-ligand dissociation. To assess the potential impact of ternary complexation on Cu partitioning into calcite in experiment 4, we measured the concentration of SRFA in both solution and precipitate samples via 3D EEM fluorescence spectroscopy. Subsequently, we calculated K_d values (Table 4) using to Equation 4. Based on this calculation SRFA was incorporated into precipitated calcite with a putative OM removal efficiency of 37%. This was consistent with the observation that the calcite precipitated in experiment 4 was significantly darker in colour compared to calcite precipitated during previous experiments. Indeed, brown colouring of speleothem calcite is known to be associated with high concentrations of OM (Blyth et al., 2007; Blyth et al., 2016; Pearson et al., 2020). The $K_{d\ SRFA}$ values determined here (average of 0.37) are presented in Table 4.

$$K_{d\,SRFA} = \frac{\left(\frac{SRFA}{Ca}\right)_s}{\left(\frac{SRFA}{Ca}\right)_{aq}} \quad (4)$$

3.4.1 Copper partitioning in the presence of SRFA

Modelled results for the SRFA experiment (Fig. 10) predicted a slow decrease in $Cu/Ca_{(aq)}$ as PCP progressed, and this was observed in our experimental data. Again, a stark contrast to the results obtained from the inorganic experiment is observed, with complexation by SRFA causing a significant decrease in Cu partitioning. The K_d value determined for the SRFA experiment was 3.3 ± 0.3 compared to 0.92 ± 0.08 for the NTA experiment, indicative of faster dissociation rates for the CuSRFA complexes, as expected due to the high stability of complexes formed with the chelating ligand NTA. The difference in K_d values observed between organic ligand experiments reported here, reinforces the importance of characterising the dissociation kinetics of divalent transition metals and OM in cave waters, before any attempt at quantitative paleohydrological interpretation using speleothems, is attempted (for context see Section 3.5).

Differences observed between model and experimental results of the SRFA experiment were deemed to result primarily from the use of an inadequate estimate of the dissociation rate of Cu-SRFA complexes (experiment 4, Fig. 10). Ternary complexation of Cu-SRFA may have also impacted the experiments; however, we found that ternary complexation could not account for the majority of the difference between modelled and observed results (see Section 3.4.2 below).

3.4.2 Partitioning of SRFA and Ternary Complexation

The $K_{d\ SRFA}$ values determined here (mean of 0.37) were consistent with the range of $K_{d\ NOM}$ values reported in the literature. Pearson et al. (2020), for instance, observed values in the range of 2.8 to 4.3 in their crystal growth study, where water from a peatland was used as the source of DOM. Hartland et al. (2014) observed average $K_{d\ NOM}$ values of 0.03 for samples taken from Pooles' Cavern, UK. The incorporation of SRFA into calcite observed here, indicated that ternary complexation may be responsible to some degree for Cu partitioning into calcite (Lee et al., 2005), therefore the partitioning of SRFA-Cu complexes was assessed according to Equation 5 (Hartland et al., 2014):

$$K_{d\ SRFA-Cu} = \frac{\left(\frac{Cu}{SRFA}\right)_s}{\left(\frac{Cu}{SRFA}\right)_{aq}} \quad (5)$$

If ternary complexation was the dominant mechanism for Cu partitioning, $K_{d\ SRFA\text{-}Cu}$ values would be ≈1, as the metal to ligand ratio would remain constant in solution and precipitate. This is a rare scenario for any complexed metal in karst systems, as ternary complexation is probably limited by the slower diffusion of NOM–M complexes relative to inorganic species, and by other complicated reaction mechanisms (e.g., steric and electrostatic effects and hydrophobic interactions between ligands). However, this mechanism has been observed for Co-NOM complexes in a hyperalkaline cave environment, due to the increased stability of Co complexes at high pH ensuring a significant decrease in dissociation rate. The whole plate $K_{d\ SRFA\text{-}Cu}$ calculated during this study (Table 4) was 9.7, indicating the ratio of Cu to SRFA in the solid was higher than in the solution, and that the dissociation kinetics of Cu-SRFA complexes rather than ternary complexation was the main factor in determining Cu availability for incorporation into calcite.

3.5 Organic Complexation and Transition Metals: Relevance for Speleothem Science

Our results demonstrate that the presence of organic matter significantly modifies the partitioning of first-row transition metals into calcite. Although the partitioning of Co, Ni and Cu can be predicted by K_d values alone in an inorganic system, this does not hold true for real-world cave systems and probably other mineral-forming environments, in which complexation by organic ligands is commonplace (e.g., Sander and Koschinsky, 2011); indeed, on Earth at least, the ubiquity of dissolved organic matter may mean that organic-mediated partitioning of metals into minerals proves to be rule, rather than the exception.

For speleothems them, although ternary complexation of NOM-M complexes may contribute to transition metal variations in speleothems, it is clear that the majority of the signal observed in speleothems results from capture of 'free' metal ions, and the formation of $Ca(M)CO_3$ solid solutions (Hartland and Zitoun, 2018). This implies that transition metal capture in speleothems generally occurs *after* the metals have dissociated from their organic host, and therefore the rate of this disintegration step becomes the key variable to resolve.

Although the use of these metals as speleothem-based proxies has generally been overlooked in favour of metals with low inorganic K_d values, in reality the widespread presence of OM in karst systems will serve to reduce the effects of PCP on these metals, and we suggest that they should be considered as valuable additions to the paleo-proxy toolbox. Our results have highlighted that the signal of these metals in speleothems is controlled by (1) the dissociation rates of the complexes, (2) the residence time of the dripwaters and (3) the inorganic partition coefficients of the metal (i.e. the compatibility of the M^{2+} ions for lattice valence sites).

With the speleothem-specific inorganic K_d values provided in this study, we now have the opportunity to assess the role of dissociation rates in speleothem trace metal signatures and isotope ratios. Given that metal supply in the presence of organic ligands follows first-order kinetics (Rate et al., 1993), we predict that the concentration of trace metals (Cu, Ni Co, and probably other metals) will be inversely related to speleothem thin-film residence times. Furthermore, we suggest Ni may be a very promising proxy given the highly similar partitioning of Ni to Ca ($K_d \sim 1$), which minimises the effects of PCP on Ni/Ca values. These findings and interpretations therefore open the possibility of using trace metal concentrations in stalagmites to reconstruct past drip rates (i.e., where thin-film residence times approximate 1/drip rate).

3.6 Experimental Limitations and Future Work

This study was performed under conditions closer to those observed in natural cave systems than have previously been achieved in laboratory-based experiments. However, in certain instances our experimental conditions deviated from natural cave environments. Notably, concentrations of trace elements were significantly higher than those observed in a natural system (where transition metals are often < 1 ppb in concentration). Although this was necessary in order to ensure sufficient concentrations for future isotope analysis, it is possible that effects that would otherwise not be observed in nature (e.g., competition between trace metals for lattice binding sites) affected the results of these experiments. This issue was mediated to some degree by ensuring X/Ca close to those observed in natural systems and metal-ligand ratios close to those reported for cave systems (Hartland and Zitoun, 2018).

Although vaterite crystals have been identified as one of the many possible initial states of speleothem crystallization (Frisia et al., 2018), it is possible that the formation of vaterite

during experiments 1-3 altered the partitioning behaviour of Co, Ni and Cu to some extent. Little data is available in the literature pertaining to the partitioning behaviour of trace elements into vaterite, and further work in this area is required to assess whether partitioning behaviour into vaterite differs markedly from calcite.

The lack of NTA concentration data for solution and precipitate samples from experiment 3 limited our ability to directly evaluate ternary complexation. However, based on the deviation between modelled and observed results, ternary complexation was unlikely to be important in this experiment. Several analytical techniques including UV-visible spectroscopy, 3D EEM fluorescence spectroscopy and Liquid Chromatography Mass Spectrometry (LC-MS) were trialled in an attempt to provide these data. However, the low concentrations of NTA coupled with matrix interferences observed for LC-MS due to high [Ca^{2+}] hampered reliable assessment of NTA concentrations. If further work on these samples were to be carried out, development of the Gas Chromatography Mass Spectrometry (GC-MS) method proposed by Reichert and Linckens (1980) to measure NTA to 1 ppb concentrations could be suitable.

To improve model accuracy of the partitioning of Co and Cu into calcite in the presence of NTA, the dissociation rate constants for CoNTA and CuNTA complexes are required. Although the modelling undertaken here effectively used the data to solve for the dissociation rate constant, confirmation that these values are in the expected range would be a valuable verification of the results.

Finally, an assessment of the isotopic fractionation of Cu in each of the experiments would be a valuable addition to the literature. It has been shown that for metals with $K_d > 1$, precipitated calcite is enriched in heavier isotopes of the trace metal (Schott et al., 2014).

Thus, it would be expected for the inorganic experiments that the precipitate would be enriched in ^{65}Cu compared to the solution. However, it is unlikely that this would be observed for the organic experiments because the organo-complexation of Cu can significantly alter the isotopic ratio of 'free' aqueous Cu species (Bigalke et. al, 2010; Ryan et al., 2014). Indeed, Schott et al. (2014) calculated that complexation of Cu by very low concentrations of oxalate ligands would suffice to ensure enrichment of calcite in light Cu instead of heavy Cu. It would be interesting to investigate the degree of fractionation observed in the presence of stronger binding organic ligands more representative of karst-derived NOM (such as SRFA), so as to help with the interpretation of Cu isotope signals present in speleothem samples.

4 CONCLUSIONS

We assessed the partitioning behaviour of Co, Ni and Cu into calcite grown under speleothem-like conditions, and determined speleothem-specific inorganic K_d values of ~ 4, 1 and 44, respectively. Their partitioning as calcite precipitation progressed was found to be predictable for the most part using the experimentally determined K_d values, when no organic ligands were present in solution. Further experiments incorporating organic ligands illustrated that the complexation of Co, Ni and Cu by organic matter significantly alters their partitioning behaviour, with apparent partition coefficients below 1 for all three metals. We demonstrated that partitioning of Co, Ni and Cu into calcite is controlled by the metal-ligand complexes, and that the amount of 'free' metal available for incorporation into calcite depends on residence time and the stability of the complexes.

This study highlights that the incorporation of the divalent first-row metals into speleothem calcite cannot not be considered in terms of simple inorganic partitioning, as the widespread

presence of NOM in karst systems will alter their partitioning behaviour significantly. Thus, although the use of these metals as speleothem-based proxies has previously been overlooked in favour of elements such as the alkali earth metals which exhibit simple partitioning (i.e., $K_d << 1$), in reality, the NOM present in karst systems will reduce the effects of PCP on these divalent first-row metals, and they should in fact be considered as useful additions to the current range of paleoenvironmental proxies. Indeed, we suggest Ni may be the most promising addition to the existing elemental proxies given 1) the widespread occurrence of Ni complexation by organic matter, and 2) the highly similar partitioning behaviour of Ni to Ca ($K_d \sim 1$) for dilute solid solutions, which minimises the effect of PCP on Ni/Ca molar ratios.

We have shown that the signal of the divalent first-row transition metals Co, Ni and Cu in speleothems will be a controlled by i) the dissociation rates (i.e. stability) of the complexes, ii) the residence time of the dripwaters and iii) the inorganic partition coefficients of the metals in question. We therefore hypothesise that transition metal partitioning into stalagmite calcite is related to the time available for metal dissociation (1/drip rate).

ACKNOWLEDGEMENTS

This research has been supported by the European Union's Horizon 2020 Research and Innovation programme through Marie Skłodowska-Curie grant (no. 691037), the Royal Society of New Zealand (grant no. RIS-UOW1501), and the Rutherford Discovery Fellowship programme (grant no. RDF-UOW1601). M. Hansen and D. Scholz acknowledge funding of the German Research Association (DFG) through grants HA 8694/1-1 and SCHO 1274/11-1.

REFERENCES

Allison, J.D., Brown, D.S. and Novo-Gradac, K.J. (1991) MINTEQA2/PRODEFA2, A geochemical model for environmental systems: Version 3.0. Office of Research and Development, U.S. Environmental Protection Agency, Washington, DC.

Amery, F., Degryse, F., Van Moorleghem, C., Duyck, M. and Smolders, E. (2010) The dissociation kinetics of Cu-dissolved organic matter complexes from soil and soil amendments. *Anal. Chim. Acta* **670**, 24-32.

Andersson, C.A. and Bro, R. (2000) The N-way toolbox for MATLAB. *Chemometr. Intell. Lab. Syst.* **52**, 1-4.

Bigalke, M., Weyer, S. and Wilcke, W. (2010) Copper isotope fractionation during complexation with insolubilized humic acid. *Environ. Sci. Technol.* **44**, 5496-5502.

Blyth, A.J., Asrat, A., Baker, A., Gulliver, P., Leng, M.J. and Genty, D. (2007) A new approach to detecting vegetation and land-use change using high-resolution lipid biomarker records in stalagmites. *Quat. Res.* **68**, 314-324.

Blyth, A.J., Hartland, A. and Baker, A. (2016) Organic proxies in speleothems: New developments, advantages and limitations. *Quat. Sci. Rev.* **149**, 1-17.

Cabaniss, S.E. (1990) pH and ionic strength effects on nickel-fulvic acid dissociation kinetics. *Environ. Sci. Technol.* **24**, 583-588.

Cabaniss, S.E. and Shuman, M.S. (1988) Copper binding by dissolved organic matter: I. Suwannee River fulvic acid equilibria. *Geochim. Cosmochim. Acta* **52**, 185-193.

Casteel, R.C. and Banner, J.L. (2015) Temperature-driven seasonal calcite growth and drip water trace element variations in a well-ventilated Texas cave: Implications for speleothem paleoclimate studies. *Chem. Geol.* **392**, 43-58.

Chakraborty, P., Manek, A., Niyogi, S. and Hudson, J. (2014) Determination of dynamic metal complexes and their diffusion coefficients in the presence of ifferent humic substances by combining two analytical techniques. *Anal. Lett.* **47**, 1224-1241.

Cheng, H., Lawrence Edwards, R., Shen, C.C., Polyak, V.J., Asmerom, Y., Woodhead, J., Hellstrom, J., Wang, Y., Kong, X., Spötl, C., Wang, X. and Calvin Alexander, E. (2013) Improvements in ^{230}Th dating, ^{230}Th and ^{234}U half-life values, and U–Th isotopic measurements by multi-collector inductively coupled plasma mass spectrometry. *Earth Planet. Sci. Lett.* **371-372**, 82-91.

Coble, P.G. (1996) Characterization of marine and terrestrial DOM in seawater using excitation-emission matrix spectroscopy. *Mar. Chem.* **51**, 325-346.

Day, C.C. and Henderson, G.M. (2013) Controls on trace-element partitioning in cave-analogue calcite. *Geochim. Cosmochim. Acta* **120**, 612-627.

Dreybrodt, W. and Scholz, D. (2011) Climatic dependence of stable carbon and oxygen isotope signals recorded in speleothems: From soil water to speleothem calcite. *Geochim. Cosmochim. Acta* **75**, 734-752.

Fairchild, I.J. and Baker, A. (2012) Speleothem Science: From Process to Past Environments. Wiley, Hoboken, UK.

Fairchild, I.J., Borsato, A., Tooth, A.F., Frisia, S., Hawkesworth, C.J., Huang, Y., McDermott, F. and Spiro, B. (2000) Controls on trace element (Sr–Mg) compositions of carbonate cave waters: implications for speleothem climatic records. *Chem. Geol.* **166**, 255-269.

Fairchild, I.J. and Hartland, A. (2010) Trace element variations in stalagmites: Controls by climate and by karst system processes, in: Stoll, H., Prieto, M. (Eds.), Ion Partitioning in Ambient Temperature Aqueous Systems: From Fundamentals to Applications in Climate Proxies and Environmental Geochemistry European Mineralogical Union, Oviedo.

Fairchild, I.J. and McMillan, E.A. (2007) Speleothems as indicators of wet and dry periods. *Int. J. Speleol.* **36**, 69-74.

Fairchild, I.J. and Treble, P.C. (2009) Trace elements in speleothems as recorders of environmental change. *Quat. Sci. Rev.* **28**, 449-468.

Fellman, J.B., Hood, E. and Spencer, R.G.M. (2010) Fluorescence spectroscopy opens new windows into dissolved organic matter dynamics in freshwater ecosystems: A review. *Limnol. Oceanogr.* **55**, 2452-2462.

Frisia, S., Borsato, A., Fairchild, I.J. and McDermott, F. (2000) Calcite fabrics, growth mechanisms, and environments of formation in speleothems from the Italian Alps and Southwestern Ireland. *J. Sediment. Res.* **70**, 1183-1196.

Frisia, S., Borsato, A. and Hellstrom, J. (2018) High spatial resolution investigation of nucleation, growth and early diagenesis in speleothems as exemplar for sedimentary carbonates. *Earth Sci. Rev.* **178**, 68-91.

Gascoyne, M. (1983) Trace-element partition coefficients in the calcite-water system and their paleoclimatic significance in cave studies. *J. Hydrol.* **61**, 213-222.

Gilmore, A.M. and Cohen, S.M. (2013) Analysis of the chromophoric dissolved organic matter in water by EEMs with Horiba-Jobin Yvon fluorescence instrument called Aqualog. *Readout* **41**, 19-24.

Giorgio, A. (1982) Critical survey of stability constants of NTA complexes. *Pure Appl. Chem.* **54**, 2693-2758.

Hansen, M., Dreybrodt, W. and Scholz, D. (2013) Chemical evolution of dissolved inorganic carbon species flowing in thin water films and its implications for (rapid) degassing of CO_2 during speleothem growth. *Geochim. Cosmochim. Acta* **107**, 242-251.

Hansen, M., Scholz, D., Froeschmann, M.L., Schöne, B.R. and Spötl, C. (2017) Carbon isotope exchange between gaseous CO_2 and thin solution films: Artificial cave experiments and a complete diffusion-reaction model. *Geochim. Cosmochim. Acta* **211**, 28-47.

Hansen, M., Scholz, D., Schöne, B.R. and Spötl, C. (2019) Simulating speleothem growth in the laboratory: Determination of the stable isotope fractionation ($\delta^{13}C$ and $\delta^{18}O$) between H_2O, DIC and $CaCO_3$. *Chem. Geol.* **509**, 20-44.

Hartland, A., Fairchild, I.J., Lead, J.R. and Baker, A. (2010) Fluorescent properties of organic carbon in cave dripwaters: Effects of filtration, temperature and pH. *Sci. Total Environ.* **408**, 5940-5950.

Hartland, A., Fairchild, I.J., Lead, J.R., Zhang, H. and Baalousha, M. (2011) Size, speciation and lability of NOM–metal complexes in hyperalkaline cave dripwater. *Geochim. Cosmochim. Acta* **75**, 7533-7551.

Hartland, A., Fairchild, I.J., Lead, J.R., Borsato, A., Baker, A., Frisia, S. and Baalousha, M. (2012) From soil to cave: Transport of trace metals by natural organic matter in karst dripwaters. *Chem. Geol.* **304-305**, 68-82

Hartland, A., Fairchild, I.J., Müller, W. and Dominguez-Villar, D. (2014) Preservation of NOM–metal complexes in a modern hyperalkaline stalagmite: Implications for speleothem trace element geochemistry. *Geochim. Cosmochim. Acta* **128**, 29-43.

Hartland, A. and Zitoun, R. (2018) Transition metal availability to speleothems controlled by organic binding ligands. *Geochem. Perspect. Lett.* **8**, 22-25.

Hering, J.G. and Morel, F.M. (1988) Humic acid complexation of calcium and copper. *Environ. Sci. Technol.***22**, 1234-1237.

Hoffmann, D.L., Prytulak, J., Richards, D.A., Elliott, T., Coath, C.D., Smart, P.L. and Scholz, D. (2007) Procedures for accurate U and Th isotope measurements by high precision MC-ICPMS. *Int. J. Mass Spectrom*. **264**, 97-109.

Hu, Q., Zhang, J., Teng, H. and Becker, U. (2012) Growth process and crystallographic properties of ammonia-induced vaterite. *MRS Online Proc. Lib.* **1272**, 3-6.

Huang, Y. and Fairchild, I.J. (2001) Partitioning of Sr^{2+} and Mg^{2+} into calcite under karst-analogue experimental conditions. *Geochim. Cosmochim. Acta* **65**, 47-62.

Irving, H. and Williams, R.J.P. (1948) Order of stability of metal complexes. *Nature* **162**, 746-747.

Ishii, S.K.L. and Boyer, T.H. (2012) Behavior of reoccurring PARAFAC components in fluorescent dissolved organic matter in natural and engineered systems: A critical review. *Environ. Sci. Technol.* **46**, 2006-2017.

Jahn, H.A. and Teller, E. (1937) Stability of polyatomic molecules in degenerate electronic states - I – Orbital degeneracy. *Proc. R. Soc. Lond. A – Math. Phys. Sci.* **161**, 220-235.

Kinniburgh, D.G., van Riemsdijk, W.H., Koopal, L.K., Borkovec, M., Benedetti, M.F. and Avena, M.J. (1999) Ion binding to natural organic matter: Competition, heterogeneity, stoichiometry and thermodynamic consistency. *Colloids Surf. A Physicochem. Eng. Asp.* **151**, 147-166.

Kitano, Y., Kanamori, N., Tokuyama, A. and Comori, T. (1973) Factors controlling the trace-element contents of marine carbonate skeletons, *Proc. Symp. Hydrogeochem. Biogeochem., Tok., Jap*. **484 - 499**.

Kitano, Y., Okumura, M. and Idogaki, M. (1980) Abnormal behaviors of copper (II) and zinc ions in parent solution at the early stage of calcite formation. *Geochem. J.* **14**, 167-175.

Lachniet, M.S. (2009) Climatic and environmental controls on speleothem oxygen-isotope values. *Quat. Sci. Rev.* **28**, 412-432.

Lakshtanov, L.Z. and Stipp, S.L.S. (2007) Experimental study of nickel(II) interaction with calcite: Adsorption and coprecipitation. *Geochim. Cosmochim. Acta* **71**, 3686-3697.

Lee, Y.J., Elzinga, E.J., Reeder, R.J., (2005) Cu (II) adsorption at the calcite–water interface in the presence of natural organic matter: kinetic studies and molecular-scale characterization. **Geochim. Cosmochim. Acta 69** (1), 49–61.Leenheer, J.A., Brown, G.K., MacCarthy, P. and Cabaniss, S.E. (1998) Models of metal binding structures in fulvic acid from the Suwannee River, Georgia. *Environ. Sci. Technol.* **32**, 2410-2416.

Lewis, G.N. (1923) Valence and the structure of atoms and molecules. The Chemical Catalog Company, inc., New York.

Lorens, R.B. (1981) Sr, Cd, Mn and Co distribution coefficients in calcite as a function of calcite precipitation rate. *Geochim. Cosmochim. Acta* **45**, 553-561.

Magiera, M., Lechleitner, F.A., Erhardt, A.M., Hartland, A., Kwiecien, O., Cheng, H., Bradbury, H.J., Turchyn, A.V., Riechelmann, S., Edwards, L. and Breitenbach, S.F.M. (2019) Local and regional Indian summer monsoon precipitation dynamics during Termination II and the Last Interglacial. *Geophys. Res. Lett.* **46**, 12454-12463.

Manceau, A. and Matynia, A. (2010) The nature of Cu bonding to natural organic matter. *Geochim. Cosmochim. Acta* **74**, 2556-2580.

Martell, A.E. and Smith, R.M. (1975) Critical Stability Constants. Plenum Press, New York and London.

Meldrum, F.C. and Hyde, S.T. (2001) Morphological influence of magnesium and organic additives on the precipitation of calcite. *J. Cryst. Growth* **231**, 544-558.

Morel, F. (1983) Principles of aquatic chemistry. Wiley, New York.

Moreno, A., Stoll, H., Jiménez-Sánchez, M., Cacho, I., Valero-Garcés, B., Ito, E. and Edwards, R.L. (2010) A speleothem record of glacial (25–11.6kyr BP) rapid climatic changes from northern Iberian Peninsula. *Glob. Planet. Change* **71**, 218-231.

Morse, J.W. and Bender, M.L. (1990) Partition coefficients in calcite: Examination of factors influencing the validity of experimental results and their application to natural systems. *Chem. Geol.* **82**, 265-277.

Mühlinghaus, C., Scholz, D. and Mangini, A. (2009) Modelling fractionation of stable isotopes in stalagmites. *Geochim. Cosmochim. Acta* **73**, 7275-7289.

Murphy, K.R., Stedmon, C.A., Graeber, D. and Bro, R. (2013) Fluorescence spectroscopy and multi-way techniques. PARAFAC. *Anal. Methods* **5**, 6557-6566.

Ni, M. and Ratner, B.D. (2008) Differentiating calcium carbonate polymorphs by surface analysis techniques – an XPS and TOF-SIMS study. *Surf. Interface Anal.* **40**, 1356-1361.

O'hara, M. and Reid, R.C. (1973) Modelling Crystal Growth Rates from Solution. Prentice-Hall, Englewood Cliffs, N.J.

Owen, R.A., Day, C.C., Hu, C.Y., Liu, Y.H., Pointing, M.D., Blättler, C.L. and Henderson, G.M. (2016) Calcium isotopes in caves as a proxy for aridity: Modern calibration and application to the 8.2 kyr event. *Earth Planet. Sci. Lett.* **443**, 129-138.

Paquette, J. and Reeder, R.J. (1995) Relationship between surface structure, growth mechanism, and trace element incorporation in calcite. *Geochim. Cosmochim. Acta* **59**, 735-749.

Parker, D.R., Norvell, W.A. and Chaney, R.L. (1995) GEOCHEM-PC - A Chemical Speciation Program for IBM and Compatible Personal Computers, Chemical Equilibrium and Reaction Models, pp. 253-269

Parkhurst, D.L. and Apello, C. (1999) User's Guide to PHREEQC Version 2. US Geological Survey 312.

Pearson, A.R., Hartland, A., Frisia, S. and Fox, B.R.S. (2020) Formation of calcite in the presence of dissolved organic matter: Partitioning, fabrics and fluorescence. *Chem. Geol.* **539**, 119492.

Pogge von Strandmann, P.A.E., Vaks, A., Bar-Matthews, M., Ayalon, A., Jacob, E. and Henderson, G.M. (2017) Lithium isotopes in speleothems: Temperature-controlled variation in silicate weathering during glacial cycles. *Earth Planet. Sci. Lett.* **469**, 64-74.

Rate, A.W., McLaren, R.G. and Swift, R.S. (1993) Response of copper(II)-humic acid dissociation kinetics to factors influencing complex stability and macromolecular conformation. *Environ. Sci. Technol.* **27**, 1408-1414.

Reichert, J.K. and Linckens, A.H.M. (1980) A simple and sensitive detection method for NTA in drinking water and river water. *Environ. Technol. Lett.* **1**, 42-49.

Rimstidt, J.D., Balog, A. and Webb, J. (1998) Distribution of trace elements between carbonate minerals and aqueous solutions. *Geochim. Cosmochim. Acta* **62**, 1851-1863.

Rostad, C.E. and Leenheer, J.A. (2004) Factors that affect molecular weight distribution of Suwannee River fulvic acid as determined by electrospray ionization/mass spectrometry. *Anal. Chim. Acta* **523**, 269-278.

Rutlidge, H., Baker, A., Marjo, C.E., Andersen, M.S., Graham, P.W., Cuthbert, M.O., Rau, G.C., Roshan, H., Markowska, M., Mariethoz, G. and Jex, C.N. (2014) Dripwater organic matter and trace element geochemistry in a semi-arid karst environment: Implications for speleothem paleoclimatology. *Geochim. Cosmochim. Acta* **135**, 217-230.

Ryan, B.M., Kirby, J.K., Degryse, F., Scheiderich, K. and McLaughlin, M.J. (2014) Copper isotope fractionation during equilibration with natural and synthetic ligands. *Environ. Sci. Technol.* **48**, 8620-8626.

Sander, S.G. and Koschinsky, A. (2011) Metal flux from hydrothermal vents increased by organic complexation. *Nat. Geosci.* **4** (3), 145-150.

Schott, J., Mavromatis, V., González-González, A. and Oelkers, E.H. (2014) Kinetic and thermodynamic controls of divalent metals isotope composition in carbonate: Experimental investigations and applications. *Procedia Earth Planet. Sci.* **10**, 168-172.

Tang, J. and Johannesson, K.H. (2003) Speciation of rare earth elements in natural terrestrial waters: assessing the role of dissolved organic matter from the modeling approach. *Geochim. Cosmochim. Acta* **67** (13), 2321-2339

Tesoriero, A.J. and Pankow, J.F. (1996) Solid solution partitioning of Sr^{2+}, Ba^{2+}, and Cd^{2+} to calcite. *Geochim. Cosmochim. Acta* **60**, 1053-1063.

Tremaine, D.M. and Froelich, P.N. (2013) Speleothem trace element signatures: A hydrologic geochemical study of modern cave dripwaters and farmed calcite. *Geochim. Cosmochim. Acta* **121**, 522-545.

Wang, Y. and Xu, H. (2001) Prediction of trace metal partitioning between minerals and aqueous solutions: A linear free energy correlation approach. *Geochim. Cosmochim. Acta* **65**, 1529-1543.

Warnken, K.W., Davison, W., Zhang, H., Galceran, J. and Puy, J. (2007) In situ measurements of metal complex exchange kinetics in freshwater. *Environ. Sci. Technol.* **41**, 3179-3185.

Wassenburg, J.A., Riechelmann, S., Schröder-Ritzrau, A., Riechelmann, D.F.C., Richter, D.K., Immenhauser, A., Terente, M., Constantin, S., Hachenberg, A., Hansen, M. and Scholz, D. (2020) Calcite Mg and Sr partition coefficients in cave environments: Implications for interpreting prior calcite precipitation in speleothems. *Geochim. Cosmochim. Acta* **269**, 581-596.

Wynn, P.M., Fairchild, I.J., Borsato, A., Spötl, C., Hartland, A., Baker, A., Frisia, S. and Baldini, J.U.L. (2018) Sulphate partitioning into calcite: Experimental verification of pH control and application to seasonality in speleothems. *Geochim. Cosmochim. Acta* **226**, 69-83.

Zhang, H. and Davison, W. (2001) In situ speciation measurements. Using diffusive gradients in thin films (DGT) to determine inorganically and organically complexed metals. *Pure Appl. Chem.* **73**, 9.

Zhang, H., Shafaei Arvajeh, M.R., Lehto, N. and Garmo, Ø.A. (2013) Kinetic studies of Ni organic complexes using Diffusive Gradients in Thin Films (DGT) with double binding layers and a dynamic numerical model. *Environ. Sci. Technol.* **47**, 463-470.

Zhang, Y. and Dawe, R.A. (2000) Influence of Mg^{2+} on the kinetics of calcite precipitation and calcite crystal morphology. *Chem. Geol.* **163**, 129-138.

Table 1

Initial composition of the experimental reservoir solutions.

Experiment	[$CaCO_3$] (mM)	[Co] (μM)	[Ni] (μM)	[Cu] (μM)	[NTA] (μM)	[SRFA] (mg l^{-1})	Initial pH	Initial Conductance (μS cm^{-1})	Initial Calcite SI
1 (Inorganic)	4.7	0.85	0.85	0.78	0	0	6.50	848	-0.01
2 (Inorganic)	5.2	0.85	0.85	0.78	0	0	6.45	848	-0.05
2 (NTA Ligand)	4.9	0.85	0.85	0.78	10.5	0	6.56	852	-0.08
3 (SRFA Ligand)	5.3	0	0	0.78	0	20	6.66	850	-0.08

Table 2

Species distributions for initial reservoir solutions modelled using visual MINTEQ 3.0 speciation codes.

		Experiment 1 (Inorganic)	Experiment 2 (Inorganic)	Experiment 3 (NTA)	Experiment 4 (SRFA)
Component	**Species**	**Proportion of Total Concentration (%)**			
Co^{2+}	Co^{2+}	70	70	7.2	-
	$CoHCO_3^+$	29	29	3	-
	$CoCO_{3\,(aq)}$	0.79	0.79	0.082	-
	Co-NTA^-	-	-	90	-
Ni^{2+}	Ni^{2+}	59	59	0.56	-
	$NiHCO^{3+}$	39	39	0.38	-
	$NiCO_{3\,(aq)}$	1.3	1.3	0.012	-
	Ni-NTA^-	-	-	99	-
Cu^{2+}	Cu^{2+}	20	20	0.019	0.79
	$CuCO_{3\,(aq)}$	71	71	0.065	2.8
	$CuNTA^-$	-	-	99.8	-
	SRFA-Cu	-	-	-	96
Ca^{2+}	Ca^{2+}	93	93	93	93
	$CaHCO_3^+$	6.6	6.6	6.6	6.5
	$CaCO_{3\,(aq)}$	0.085	0.085	0.085	0.084
	Ca-NTA^-	-	-	-	-
	SRFA-Ca	-	-	-	0.26
CO_3^{2-}	$CaHCO^{3+}$	1.8	1.8	1.8	1.8
	$CaCO_{3\,(aq)}$	0.024	0.024	0.024	0.024
	HCO_3^-	54	54	54	54
	$CO_{2\,(aq)}$	44	44	44	44

Table 3

Partition coefficients calculated for Co, Ni and Cu during inorganic experiments 1 and 2. Errors were calculated from the standard deviation of triplicate ICP-MS measurements.

Experiment 1						Experiment 2					
Distance of Flow (cm)	**Residence Time (s)**	**PCP (%)**	**K_d**			**Distance of Flow (cm)**	**Residence Time (s)**	**PCP (%)**	**K_d**		
			Co	**Ni**	**Cu**				**Co**	**Ni**	**Cu**
2 ± 0.5	6 ± 0.56	0	2.6 ± 0.2	0.75 ± 0.05	34 ± 3	5 ± 0.5	14 ± 0.53	0	1.80 ± 0.3	0.35 ± 0.07	< QL
7 ± 0.5	21 ± 2.0	7.9 ± 0.2	2.5 ± 0.1	0.46 ± 0.03	60 ± 2	9 ± 0.5	26 ± 1.0	10.5 ± 0.5	1.97 ± 0.1	0.27 ± 0.02	< QL
12 ± 0.5	35 ± 3.4	11.5 ± 0.4	3.0 ± 0.2	0.55 ± 0.03	120 ± 7	12 ± 0.5	34 ± 1.3	13.0 ± 0.5	2.49 ± 0.5	0.32 ± 0.07	< QL
17 ± 0.5	50 ± 4.8	15.0 ± 0.6	6.0 ± 0.3	1.1 ± 0.07	< QL	17 ± 0.5	48 ± 1.8	16.7 ± 0.7	2.80 ± 0.2	0.31 ± 0.03	< QL
27 ± 0.5	79 ± 7.6	21.6 ± 0.4	8.8 ± 0.3	1.5 ± 0.04	< QL	-	-	-	-	-	-
37 ± 0.5	109 ± 10	27.0 ± 1.1	9.7 ± 1.1	1.6 ± 0.15	< QL	37 ± 0.5	105 ± 3.9	25.6 ± 1.4	5.92 ± 0.6	0.76 ± 0.08	< QL
47 ± 0.5	138 ± 13	32.2 ± 1.2	8.7 ± 0.5	1.4 ± 0.06	< QL	47 ± 0.5	134 ± 5.0	28.0 ± 1.7	7.87 ± 0.7	0.98 ± 0.08	< QL
57 ± 0.5	168 ± 16	35.1 ± 0.9	7.8 ± 0.6	1.4 ± 0.07	< QL	-	-	-	-	-	-
67 ± 0.5	197 ± 19	39.1 ± 1.6	8.5 ± 1.1	1.6 ± 0.20	< QL	67 ± 0.5	191 ± 7.1	34.2 ± 1.6	7.09 ± 0.6	1.08 ± 0.10	< QL
85 ± 0.5	250 ± 24	47.0 ± 1.9	3.7 ± 0.2	0.96 ± 0.05	< QL	85 ± 0.5	242 ± 9.0	36.2 ± 1.8	12.46 ± 1.0	1.30 ± 0.11	< QL
	K_d for Entire Plate:		**4.4 ± 0.3**	**1.1 ± 0.1**	**44 ± 3**		**K_d for Entire Plate:**		**3.6 ± 0.5**	**0.7 ± 0.01**	**< QL**

Table 4

Partition coefficients calculated during organic experiments 3 and 4. Errors were calculated from the standard deviation of triplicate ICP-MS measurements.

Experiment 3 (NTA)						Experiment 4 (SRFA)					
Distance of Flow (cm)	**Residence Time (s)**	**PCP (%)**	**K_d**			**Distance of Flow (cm)**	**Residence Time (s)**	**PCP (%)**	**K_d**		
			Co	**Ni**	**Cu**				**Cu**	**SRFA**	**SRFA-Cu**
5 ± 0.5	23 ± 0.8	0	0.38 ± 0.03	0.06 ± 0.009	0.78 ± 0.07	-	-	-	-	-	-
9 ± 0.5	41 ± 1.4	4.5 ± 0.3	0.36 ± 0.03	0.02 ± 0.005	0.78 ± 0.06	-	-	-	-	-	-
12 ± 0.5	54 ± 1.8	7.4 ± 0.4	0.43 ± 0.04	0.08 ± 0.012	0.94 ± 0.1	-	-	-	-	-	-
17 ± 0.5	77 ± 2.6	9.5 ± 0.8	0.46 ± 0.03	0.02 ± 0.005	1.01 ± 0.07	-	-	-	-	-	-
27 ± 0.5	122 ± 4.1	13.5 ± 1.0	0.45 ± 0.04	0.02 ± 0.006	1.04 ± 0.11	-	-	-	-	-	-
37 ± 0.5	167 ± 5.6	16.2 ± 1.2	0.47 ± 0.04	0.02 ± 0.006	1.09 ± 0.07	37 ± 0.5	99 ± 15	10.5 ± 0.2	3.4 ± 0.1	-	-
47 ± 0.5	212 ± 7.1	23.7 ± 1.9	0.39 ± 0.03	0.02 ± 0.004	0.93 ± 0.07	47 ± 0.5	126 ± 19	12.3 ± 0.2	4.5 ± 0.1	0.44	10.3
57 ± 0.5	257 ± 8.6	25.7 ± 2.1	0.35 ± 0.03	0.02 ± 0.006	0.88 ± 0.09	57 ± 0.5	153 ± 23	11.4 ± 0.3	3.3 ± 0.4	0.35	9.4
67 ± 0.5	302 ± 10	29.9 ± 1.6	0.34 ± 0.02	0.02 ± 0.007	0.85 ± 0.05	65 ± 0.5	175 ± 26	11.9 ± 0.3	3.1 ± 0.4	0.34	9.2
89 ± 0.5	401 ± 14	34.1 ± 3.3	0.35 ± 0.03	0.02 ± 0.006	0.83 ± 0.07	85 ± 0.5	228 ± 34	16.5 ± 0.4	2.7 ± 0.1	-	-
K_d for Entire Plate:			**0.41 ± 0.03**	**0.029 ± 0.007**	**0.92 ± 0.08**	**K_d for Entire Plate:**			**3.3 ± 0.3**	**0.37**	**9.7**

Table 5

Selected literature K_d values for partitioning of Co, Ni and Cu into calcite.

	K_d	Reference
Co^{2+}	1.9	Day and Henderson (2013)
	8.4	Lorens (1981)
	9.3	Wang and Xu (2001)
	10.9	Rimstidt et al. (1998)
Ni^{2+}	0.2	Rimstidt et al. (1998)
	~1	Stipp and Lakshtanov (2007)
	3.5	Wang and Xu (2001)
Cu^{2+}	80.2	Rimstidt et al. (1998)
	37.2	Wang and Xu (2001)
	25	Kitano et al. (1973)
	23.3	Kitano et al. (1980)